Nucl. Phys. B 1029 (2026) 117521

Contents lists available at ScienceDirect

Nuclear Physics, Section B

journal homepage: www.elsevier.com/locate/nuclphysb

Localized helical spin texture in ferromagnetic thin films

Xiao-Qi Cui [a,b], Xin-Wei Jin [c], Shiyi Wang [a,b], Xiao-Yong Wen [d], Zhan-Ying Yang [a,b,e,*]

[a] School of Physics, Northwest University, Xi'an, 710127, China
[b] Peng Huanwu Center for Fundamental Theory, Xi'an, 710127, China
[c] Department of Physics, Zhejiang Normal University, Jinhua, 321004, China
[d] School of Applied Science, Beijing Information Science and Technology University, Beijing, 100192, China
[e] Shaanxi Key Laboratory for Theoretical Physics Frontiers, Xi'an, 710127, China

ARTICLE INFO

Editor: Olalla Castro Alvaredo

Keywords:
Localized helical spin texture
Chiral magnetic excitation
Gauge equivalence

ABSTRACT

Based on a continuous spin dynamics model of two-dimensional ferromagnetic thin films, we employ a gauge equivalence approach to transform the spin dynamical equations into analytically tractable scalar forms, establishing a constructive framework that directly links spin dynamics to real-space spin configurations. Within this framework, we construct and analyze localized helical spin textures, whose magnetization is confined within a finite spatial region while the spin orientation undergoes continuous rotation, giving rise to a well-defined chirality. These textures can be classified into three fundamental types: left-handed helices, right-handed helices, and mixed helices. We further show that multiple localized helical textures can coexist and form composite configurations under nonlinear dynamical constraints, leading to distinct bound states composed of textures with the same or opposite chirality. These results identify localized helical spin textures as a class of fundamental nonlinear magnetic excitations in two-dimensional ferromagnetic systems, and provide a concrete analytical route for understanding the emergence and combination of chiral spin structures beyond periodic magnetic order.

1. Introduction

In magnetic systems, the spatial arrangement of spin degrees of freedom is far richer than that of uniform magnetic order, giving rise to a variety of nonuniform magnetization configurations collectively referred to as spin textures, including domain walls, magnetic vortices, magnetic bubbles, and skyrmions [1–3]. These structures can be stabilized by topological constraints or nonlinear dynamical mechanisms, and they share the common feature that the spin orientation varies continuously in space, which fundamentally distinguishes them from simple ferromagnetic or antiferromagnetic ground states [4–6]. More generally, spin textures provide a fundamental platform for the coupling between nonlinear effects and spatial structures in magnetic systems, serving as an essential entry point for understanding complex magnetic excitations and multiscale magnetization dynamics [7,8]. Moreover, spin textures are not merely geometric modulations of magnetic order, but also act as carriers of energy, momentum, and information [9,10]. In ferromagnetic thin films and interfacial systems, they can be driven into controlled motion by external fields, electric currents, or temperature gradients, thereby exhibiting promising potential for applications in spintronics as information bits, energy transport channels, and nonlinear magnetic excitations [11–16]. Consequently, identifying new types of spin textures and gaining a deeper

* Corresponding authors.
E-mail addresses: jinxinwei@zjnu.edu.cn (X.-W. Jin), zyyang@nwu.edu.cn (Z.-Y. Yang).

https://doi.org/10.1016/j.nuclphysb.2026.117521
Received 10 February 2026; Received in revised form 20 May 2026; Accepted 22 May 2026
Available online 23 May 2026

understanding of their formation mechanisms, structural characteristics, and dynamical behaviors has remained one of the central issues in magnetic research.

Among the known spin textures, helical structures occupy a fundamental yet distinctive position, describing chiral magnetic states in which spins continuously rotate along a specific spatial direction [17,18]. Such configurations can serve either as background states for complex topological structures, such as skyrmion lattices, or as standalone manifestations of how chiral interactions regulate magnetic order, and they possess unique physical significance in spin transport, nonreciprocal propagation, and the control of magnetic excitations [19,20]. However, most helical textures investigated to date are periodic or quasiperiodic magnetic orders that extend throughout the entire system and rely on specific mechanisms, such as the Dzyaloshinsky-Moriya interaction or broken lattice symmetries [21–24]. Such helices are difficult to confine spatially and therefore are not well suited as localized carriers of magnetic information or energy. In addition, analytical descriptions of the coexistence, interaction, or superposition of distinct helical states remain limited, which restricts their controllable manipulation and functional implementation. These limitations highlight the importance of spatially localized helical spin textures in two-dimensional ferromagnetic systems, which preserve a well-defined helical chirality without relying on extended periodic magnetic order and enable controlled chiral magnetic excitations beyond conventional periodic helical structures. Their intrinsic spatial localization further suggests potential applications as localized carriers of magnetic information or energy.

The present work is devoted to addressing this question. Based on the continuous Heisenberg model for two-dimensional ferromagnetic thin films, we employ a gauge-equivalence approach to construct a class of spin textures that simultaneously possess helical chirality and spatial localization. These structures appear as magnetization patterns restricted to finite spatial regions, with spins undergoing smooth spatial rotation, and can be classified into three fundamental types of localized helical spin textures: left-handed, right-handed, and mixed helices. They can be regarded as the basic building blocks of localized helical magnetic excitations in two-dimensional ferromagnetic systems. Our results address the spatial confinement limitations of previously studied periodic and quasiperiodic helices, showing that localized helices could potentially carry magnetic information or energy and providing concrete examples for investigating chiral spin interactions, superpositions, and controllable manipulation. The remainder of this paper is organized as follows. In Section 2, the model and methods are introduced. In Section 3, the classification of localized helical spin textures and their composite forms is presented, together with a discussion of the corresponding chiral magnetic excitations. Finally, the main results are summarized and discussed.

2. Continuous spin dynamics and gauge equivalent formulation

We consider spin dynamics in two-dimensional ferromagnetic thin films within a continuous description of the magnetization field. In this section, we introduce the effective spin dynamical equations and then recast them, for analytical convenience, into a gauge-equivalent form that will be used throughout the following sections.

2.1. A two-dimensional continuous Heisenberg ferromagnet model

The following Heisenberg ferromagnet spin field equation [25–27] describes continuous spin dynamics in two spatial dimensions:

$$\begin{aligned} &\vec{S}_t = (\vec{S}\times\vec{S}_y + u\vec{S})_x + v_1\vec{S}_x, \\ &u_x = -\vec{S}\cdot(\vec{S}_x\times\vec{S}_y), \end{aligned} \tag{1}$$

where $\vec{S}=(S^x,S^y,S^z)$ is the spin vector field, satisfying $|\vec{S}|=1$, and $u(x,y,t)$ is a scalar field determined self-consistently by the spin configuration. The model characterizes the continuous dynamical behavior of spin configurations in two-dimensional ferromagnetic systems, in which the time evolution of the magnetization is naturally confined to the unit sphere, allowing the spin orientation to vary continuously in space. The first term $(\vec{S}\times\vec{S}_y)_x$ represents an exchange-induced rotational contribution originating from spatial variations along the transverse y direction, whose effect is dynamically transmitted through the derivative with respect to x. This term introduces an intrinsic anisotropy into evolution, whereby rotational features generated in one spatial direction are propagated and modulated along another. The scalar field $u(x,y,t)$ is defined through the auxiliary relation $u_x=-\vec{S}\cdot(\vec{S}_x\times\vec{S}_y)$, where the quantity $\vec{S}\cdot(\vec{S}_x\times\vec{S}_y)$ is a scalar geometric density characterizing the local twisting of the two-dimensional spin configuration. Although u itself is a scalar field, its coupling to the vector field $\vec{S}$ through the term $u\vec{S}$ modifies the spin dynamics in a geometry-dependent manner. The contribution $u\vec{S}$ acts as a longitudinal modulation of the spin evolution and introduces a coupling between the local geometric structure of the magnetization field and its dynamical behavior. The term $v_1\vec{S}_x$ corresponds to a convective contribution, describing a uniform translational motion of the spin configuration along the x-direction. This term does not affect the internal rotational structure of the spin texture, but it shifts the propagation characteristics of localized excitations.

Next, we will present the linear spectral problem for Eq. (1) as follows:

$$\begin{aligned} &\Phi_x = \Gamma\Phi = \frac{\mathrm{i}}{2}\lambda\mathrm{S}\Phi, \\ &\Phi_t = \lambda\Phi_y + \Xi\Phi = \lambda\Phi_y + \frac{\lambda}{4}\{[\mathrm{S},\mathrm{S}_y] + 2\mathrm{i}(v_1+u)\mathrm{S}\}\Phi, \end{aligned} \tag{2}$$

in which

$$[\mathrm{S},\mathrm{S}_y] = \mathrm{S}\cdot\mathrm{S}_y - \mathrm{S}_y\cdot\mathrm{S}, \quad \mathrm{S} = \begin{pmatrix} S^z & S^- \\ S^+ & -S^z \end{pmatrix}, \quad S^\pm = S^x \pm \mathrm{i}S^y.$$

The matrix S can also be written as $\mathrm{S} = S^x\sigma_1 + S^y\sigma_2 + S^z\sigma_3$, where σ_1, σ_2 and σ_3 denote the Pauli matrices. The spectral parameter λ satisfies the nonlinear constraint $\lambda_t - \lambda\lambda_y = 0$ and $\lambda_x = 0$. Lax pair (2) provides Eq. (1) with the compatibility condition $\Gamma_t - \Xi_x + \Gamma\Xi - \Xi\Gamma - \lambda\Gamma_y = 0$, and the eigenvector $\Phi = (\phi_1(x, y, t, \lambda), \phi_2(x, y, t, \lambda))^{\mathrm{T}}$ must meet $\Phi_{xt} = \Phi_{tx}$ and $\Phi_{xy} = \Phi_{yx}$.

When $\nu_1 = 0$, we note that Eq. (1) corresponds to the well-known Myrzakulov-I (M-I) spin equation and reduces to the classical continuum Heisenberg ferromagnet equation $\vec{S}_t = \vec{S} \times \vec{S}_{xx}$, which may be viewed as the integrable nondissipative limit of the Landau-Lifshitz-Gilbert (LLG) equation with spin-transfer torque under standard micromagnetic scaling. More generally, the corresponding LLG-type dynamics can be written as $\frac{\partial \mathbf{m}}{\partial \tau} = \mathbf{m} \times \mathbf{m}_{\zeta\zeta} + \alpha\mathbf{m} \times (\mathbf{m} \times \mathbf{m}_{\zeta\zeta}) + \mathcal{Q}\mathbf{m}_{\zeta}$ [18,27], where α and $\mathcal{Q}$ denote the Gilbert damping and spin-transfer torque strength, respectively. The equation $\vec{S}_t = \vec{S} \times \vec{S}_{xx}$ corresponds to the special case $\alpha = 0$ and $\mathcal{Q} = 0$. In this sense, the present two-dimensional model may be regarded as a nonlinear continuous spin-field extension that preserves the essential rotational spin dynamics of the classical Heisenberg ferromagnet framework.

Since the present work mainly focuses on nonlinear dynamical structures of the dimensionless two-dimensional spin system rather than on material-specific micromagnetic modeling, all results are presented in normalized units. Nevertheless, to provide an approximate physical scale reference, one may borrow the standard scaling relations of the one-dimensional Heisenberg ferromagnet model. Using typical permalloy parameters, the characteristic scales are estimated to be on the order of $1\,\zeta \approx 5.68$ nm, $1\,\tau \approx 5.7$ ps.

These estimates are intended only to provide representative physical magnitude references for the dimensionless variables used in the present work, rather than a strict material-specific mapping of the two-dimensional model considered here. Overall, this two-dimensional continuous dynamical model offers a consistent framework for studying nonuniform spin configurations with internal rotational structures in ferromagnetic thin films.

2.2. Gauge equivalence and analytical representation of spin textures

The two-dimensional Heisenberg ferromagnetic spin field model considered here is formulated as a continuous vector field equation. Direct analytical treatment is generally nontrivial, as the presence of multiple spatial directions significantly increases the gauge and geometric complexity compared with one-dimensional systems, where the gauge equivalent method has been effectively used to relate the spin equation to a scalar integrable equation [28,29]. In two dimensions, the compatibility conditions must be satisfied simultaneously along different directions, and the resulting scalar equations are typically more intricate. In this work, we extend the gauge equivalent approach to the two-dimensional case, establishing a correspondence between the original vector spin equation and an associated scalar system, which provides a more tractable framework for analytical investigations.

For the two-dimensional spin field Eq. (1), previous studies have merely proven, based on geometric equivalence arguments, that it is gauge equivalent to a scalar equation [30–33]:

$$\mathrm{i}\psi_t - \psi_{xy} - V\psi = 0, \quad V_x = 2\partial_y|\psi|^2. \tag{3}$$

with its corresponding Lax pair provided:

$$\begin{aligned} &\Psi_x = \mathrm{U}\Psi = \left(\frac{\mathrm{i}\lambda}{2}\sigma_3 + Q\right)\Psi, \\ &\Psi_t = \lambda\Psi_y + \mathrm{V}\Psi = \lambda\Psi_y - \mathrm{i}\sigma_3\left(\frac{V\mathrm{E}}{2} + Q_y\right)\Psi, \end{aligned} \tag{4}$$

where $\lambda_x = 0$, $\lambda_t = \lambda\lambda_y$ and

$$V = 2\partial_x^{-1}\partial_y(|\psi|^2), \quad \mathrm{E} = \begin{pmatrix} 1 & 0 \\ 0 & 1 \end{pmatrix}, \quad Q = \begin{pmatrix} 0 & \psi \\ -\psi^* & 0 \end{pmatrix}.$$

For Eq. (1), previous studies have primarily employed gauge equivalence to clarify the structural and integrability properties of the dynamical equations. While such equivalence proves a formal correspondence with scalar-field models, it does not provide a practical procedure to reconstruct the full three-component spin vector from scalar wave functions. In the present work, we address this limitation by starting from the scalar-field equation and employing an explicit gauge transformation to recover the complete spin vector field. This approach enables direct construction of spatially structured spin configurations from scalar solutions. In this context, gauge equivalence acts as an analytic bridge connecting scalar solutions to the spin field. Specifically, we consider the gauge transformation $\Psi = G(x, y, t)\Phi$ and utilize the associated spectral problem (4), which yields

$$\Psi_x = G_x\Phi + G\Gamma\Phi = \mathrm{U}G\Phi, \tag{5}$$

Eq. (5) implies:

$$G_xG^{-1} + \frac{\mathrm{i}\lambda}{2}G\mathrm{S}G^{-1} = Q + \frac{\mathrm{i}\lambda}{2}\sigma_3. \tag{6}$$

We then take $G = G(x, y, t)$ to be the matrix solution of the spectral problem (4) evaluated at $\lambda = 0$, which serves as the seed for reconstructing the spin configuration. Accordingly, G satisfies

$$G_x = \mathrm{U}|_{\lambda=0}G \triangleq \mathrm{U}(0)G, \quad G_t = \Psi_t|_{\lambda=0}G \triangleq \mathrm{V}(0)G. \tag{7}$$

From the structure of U(0) and V(0), the undetermined matrix G in (7) can be expressed as

$$G = \begin{pmatrix} \mathcal{F}(x, y, t) & -\mathcal{G}^*(x, y, t) \\ \mathcal{G}(x, y, t) & \mathcal{F}^*(x, y, t) \end{pmatrix}. \tag{8}$$

Based on (6), we can deduce that

$$G_x = QG = \mathrm{U}(0)G, \tag{9a}$$

$$S^x = -\frac{\mathcal{F}^*\mathcal{G}^* + \mathcal{G}\mathcal{F}}{|\mathcal{F}|^2 + |\mathcal{G}|^2}, \quad S^y = -\mathrm{i}\frac{\mathcal{F}^*\mathcal{G}^* - \mathcal{G}\mathcal{F}}{|\mathcal{F}|^2 + |\mathcal{G}|^2}, \quad S^z = \frac{|\mathcal{F}|^2 - |\mathcal{G}|^2}{|\mathcal{F}|^2 + |\mathcal{G}|^2}. \tag{9b}$$

The expression in (9a) is consistent with the relation in (7). Using (7) together with (8), the $\mathcal{F}$ and $\mathcal{G}$ in (9b) satisfy the following relations:

$$\mathcal{F}_x = \psi_\iota \mathcal{G}, \quad \mathcal{G}_x = -\psi_\iota \mathcal{F}, \quad \iota = 1, 2 \cdots N, \tag{10}$$

where ψ_ι represents the exact solution of the scalar equation, the subscript ι represents the ι-soliton solution. The time relationship still satisfies the above deduction. It therefore follows that the two-dimensional ferromagnetic spin Eq. (1) and the scalar Eq. (3) are gauge equivalent, and that explicit spin texture configurations can be directly reconstructed from analytic solutions of the scalar equation, as shown in Eq. (9b). In this sense, the gauge transformation here serves not only as a formal equivalence, but also as a constructive tool for generating concrete spin configurations.

3. Localized helical spin textures and their composite structures

Building on the gauge-equivalence framework introduced in Section 2.2, we now turn to the construction and analysis of specific spin configurations in two-dimensional ferromagnetic thin films. This framework enables the systematic generation of spatially structured spin fields from analytic scalar solutions. In the following, we examine the resulting spin textures, focusing on their spatial distribution characteristics, internal rotational characteristics, and possible composite forms.

3.1. Chiral helical classification and basic localized helical spin textures

First, by applying the Darboux transformation in Appendix A, when $N = 1$ and $\lambda_1 = a_1 + b_1\mathrm{i}$, we obtain the wave-function representation of the scalar Eq. (3) in the form

$$\psi_1 = b_1 \operatorname{sech}(\xi)\mathrm{e}^{\mathrm{i}\delta}, \tag{11}$$

where $\xi = b_1 x - \frac{2a_1}{a_1^2+b_1^2} y - 2t$ and $\delta = a_1 x - \frac{2b_1}{a_1^2+b_1^2} y$. According to (9)–(11), the following relationship can be derived through integration operations:

$$\begin{aligned} S^x &= -\frac{2}{a_1^2 + b_1^2} b_1 \operatorname{sech}^2(\xi)\left[a_1 \sin(\delta)\cosh(\xi) + b_1 \cos(\delta)\sinh(\xi)\right], \\ S^y &= -\frac{2}{a_1^2 + b_1^2} b_1 \operatorname{sech}^2(\xi)\left\{a_1 \cos(\delta)\cosh(\xi) - b_1 \sin(\delta)\sinh(\xi)\right\}, \\ S^z &= 1 - \frac{2}{a_1^2 + b_1^2} b_1^2 \operatorname{sech}^2(\xi), \quad \vec{S} = (S^x, S^y, S^z). \end{aligned} \tag{12}$$

The relationship between the three components and the wave function is as follows

$$S^+ = \frac{2\mathrm{e}^{-2\mathrm{i}\delta}}{|\lambda_1|^2}\psi_1\left[b_1 \tanh(\xi) + \mathrm{i}a_1\right], \quad S^- = \frac{2}{|\lambda_1|^2}\psi_1\left[b_1 \tanh(\xi) - \mathrm{i}a_1\right], \quad S^z = 1 - \frac{2}{|\lambda_1|^2}|\psi_1|^2. \tag{13}$$

To characterize the spatial distribution features of spin textures, we introduce the polar angle θ and the azimuthal angle φ as two independent variables to reparameterize the three spin components in (12). Here, θ is defined as the angle between the spin and the z axis, while φ is the angle between the projection of the spin onto the xy plane and the x axis. The relevant information can be seen in the lower-left corner of Fig. 1(a1). Using the spin vector with $|\vec{S}| = 1$, we then define

$$\mathcal{J} = S^x + \mathrm{i}S^y = \sin(\theta)\,\mathrm{e}^{\mathrm{i}\varphi}, \quad S^z = \cos(\theta). \tag{14}$$

Substituting (12) into (14) yields the corresponding representation in terms of the angular variables. In particular, we obtain $\mathcal{J} = -\frac{2b_1\,\mathrm{e}^{-\mathrm{i}\delta}\,\operatorname{sech}(\xi)\left(a_1\mathrm{i}+b_1\tanh(\xi)\right)}{a_1^2+b_1^2}$, where the phase factor prevents $\mathcal{J}$ from directly reflecting the correct local phase information. To eliminate this contribution, we introduce the following modified quantity:

$$\widetilde{\mathcal{J}} = \mathcal{J}\mathrm{e}^{\mathrm{i}\delta}, \tag{15}$$

which effectively eliminates the periodic background phase and retains only the physically relevant local phase information. The azimuthal angle is then given by $\varphi = \arg(\widetilde{\mathcal{J}})$, characterizing the spatial winding of the spin in the transverse plane, while the polar angle $\theta = \arccos(S^z)$ measures the deviation of the spin from the uniform ferromagnetic background. These two angle variables jointly determine the helical characteristics of spin texture, and their representative configurations are shown in Fig. 1(a1) and (b1), respectively. As an example, in Fig. 1(a1), along the x-axis, the polar angle θ of the spins initially aligns with the z axis, gradually perpendicular to the z axis, and finally returns toward alignment with the z axis. Meanwhile, the azimuthal angle φ decreases

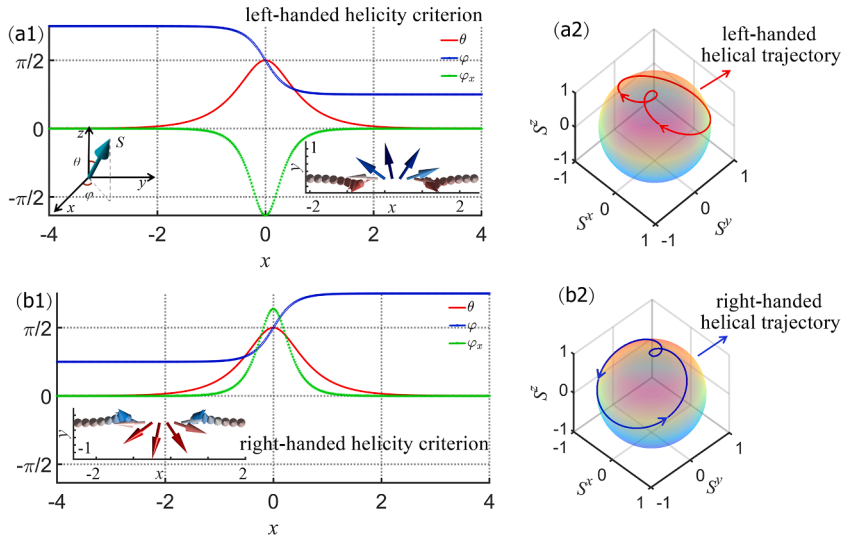

Fig. 1. (Color online) Chiral helical classification. (a1) and (b1) display the chiral helical and their spatial distribution features by the polar angle, azimuthal angle, and phase gradient flow. (a2) and (b2) correspondingly show the trajectories of the three components of the spin texture on the Bloch sphere, whose geometric forms follow the left-handed and right-handed helical rules, respectively. The relevant parameters are: (a1)-(a2) $\lambda_1 = 2 - 2\mathrm{i}$, (b1)-(b2) $\lambda_1 = -2 - 2\mathrm{i}$, $y = t = u_0 = -v_1 = t = 0$.

gradually, indicating that, when viewed from above, the spin rotates clockwise in the xy plane. In contrast, Fig. 1(b1), the rotation direction in the xy plane is reversed, illustrating the helical nature of the spin textures.

Although the helical characteristics of spin texture can be qualitatively distinguished from the angular representation in terms of the polar and azimuthal angles, a more rigorous and quantitative criterion is required to unambiguously characterize their helical direction. To this end, we introduce a helicity index based on the phase-gradient flow of the azimuthal angle, referred to as the chirality index, which provides criteria for determining left-handed and right-handed helices. Specifically, we evaluate the spatial derivative of the azimuthal angle φ along the x direction at $y = 0$, namely $\partial_x \varphi|_{y=0}$,

$$\varphi_x = -\frac{a_1 b_1^2}{a_1^2 \cosh^2(b_1 x) + b_1^2 \sinh^2(b_1 x)}. \tag{16}$$

Together, these parameters control the spatial localization and dynamical evolution of the helical spin configuration, and the sign of φ_x provides a direct quantitative measure of the local rotational sense of the spin texture. The sign of this quantity provides a natural and intrinsic criterion for distinguishing between left-handed and right-handed helices. This phase-gradient flow is explicitly controlled by the system parameters a_1, thus allowing us to determine the chiral helicity index as $\mathcal{I} = \mathrm{sgn}(\int \nabla\varphi dr) = \mathrm{sgn}(a_1) = \pm 1$. This criterion is equivalent to the commonly used definition of chirality in spin textures based on the triple vector product $Z = \mathbf{n} \cdot (S^x \times S^y)$, where $\mathbf{n}$ is a geometry-related reference direction, and S^x and S^y denote the magnetization directions at two neighboring positions within the spin texture. The sign of Z directly characterizes the rotational chirality of the spin texture. The determination of the chiral helical index is illustrated by the green curves in Fig. 1(a1) and (b1). To clarify this classification criterion, we map the spin textures onto the Bloch sphere for visualization, where the corresponding trajectories on the sphere exhibit left-handed or right-handed helical structures, as shown in Fig. 1(a2) and (b2).

Through the qualitative and quantitative analysis based on the polar angle, azimuthal angle, and phase-gradient flow, we have established a criterion for judging chiral helical features. The spin textures composed of three components are visualized as shown in Fig. 2. It can be clearly observed that, at $a_1 = -b_1$, the spatial spin configuration exhibits left-handed helical characteristics, and this structure is thus referred to as a left-handed localized helical spin texture, as shown in Fig. 2(a1). Similarly, for $a_1 = b_1$, the configuration corresponds to a right-handed localized helical spin texture, as shown in Fig. 2(a2). In contrast, when $a_1 \neq \pm b_1$, the phase-gradient flow changes sign in different spatial regions, indicating the coexistence of left- and right-handed helical components within a single localized structure. Such configurations are therefore referred to as mixed localized helical spin textures, as illustrated in Fig. 2(b1) and (b2). At this point, we provide three basic types of localized helical spin textures and their judgment criteria in this system.

To further elucidate the structure of the localized helical spin textures, the spatial profiles of the three spin components corresponding to left-handed, right-handed, and mixed helices are displayed in Fig. 2. It is observed that for the symmetric cases $a_1 = \mp b_1$, the transverse components S^x and S^y exhibit characteristic inverted N-shaped and W, M-shaped profiles, while the longitudinal component S^z forms a standard dark-soliton-like structure, as shown in Fig. 2(c1)-(d3). As time evolves, the overall motion of the localized structure follows a uniform drift with velocity $\vec{v} = \frac{-2}{b_1^2+q^2}(-b_1, q)$, where $q = \frac{2a_1}{a_1^2+b_1^2}$. During this evolution, the profile of S^z remains essentially unchanged apart from translation, whereas the transverse components S^x and S^y undergo continuous shape modulation.

Importantly, this continuous variation of S^x and S^y does not arise merely from the algebraic superposition of trigonometric and hyperbolic functions in the analytical expressions. Instead, it reflects the interplay between two distinct structural contributions: a spatially uniform rotational background encoded in the phase factor δ, which was previously removed through the definition $\widetilde{\mathcal{J}}$, and a localized chiral excitation associated with the soliton envelope $\mathrm{sech}(\xi)$. As the system evolves in time, the localized chiral rotation is continuously superimposed onto the background spin rotation, leading to periodic deformation of the transverse spin profiles while preserving spatial localization. When $a_1 \neq \pm b_1$, the competition between these two contributions becomes more pronounced, resulting in spin configurations whose three components exhibit breathing-like behavior, as illustrated in Fig. 2(e1)-(e3). These structures therefore represent mixed localized helical spin textures, in which left- and right-handed rotational features coexist within a single localized excitation.

Taking the three components of left-handed localized helical spin texture as an example. We further present in Fig. 3 the temporal evolution of the three spin components S^x, S^y, and S^z. The results confirm that, consistent with the analytical expressions, the transverse components S^x and S^y undergo continuous structural variation during time evolution, whereas the profile of S^z remains invariant. This behavior provides additional evidence that spin textures with the same chirality may nevertheless exhibit distinct spatial distribution characteristics.

Based on the above analysis, within the gauge equivalence framework, the scalar analytical solutions can be used to explicitly construct three-component spin fields. The helical features of localized spin textures can be clearly characterized through the polar angle, azimuthal angle, and phase gradient flow, and their three-component structure can be analyzed, allowing the distinction of three basic types of textures. A natural question then arises: when multiple such textures coexist, how do they maintain their individual structures and interact under nonlinear constraints? This issue will be addressed in the next section.

3.2. Composite multi-excitation states of localized helical spin textures

When $N = 2$, $\lambda_1 = a_1 + b_1\mathrm{i}$ and $\lambda_2 = a_2 + b_2\mathrm{i}$, with the help of 2-fold DT, we can obtain the wave-function representation of the scalar-field Eq. (3)

$$\psi_2 = \frac{\mathcal{R}_1}{\mathcal{R}_2}, \tag{17}$$

with

$$\begin{aligned}
&\mathcal{R}_1 = (b_1^2 - b_2^2)(r_1 b_1 \mathrm{e}^{-5\xi_{1\mathfrak{I}}+4\xi_{2\mathfrak{I}}} + r_2 \mathrm{e}^{-4\xi_{1\mathfrak{I}}+3\xi_{2\mathfrak{I}}} + r_3),\\
&\mathcal{R}_2 = \left[r_4 \mathrm{e}^{-2\xi_{1\mathfrak{I}}+2\xi_{2\mathfrak{I}}} + r_5 b_1^2 \sinh(\xi_{1\mathfrak{R}})\right](r_5 b_1 b_2 + r_6 \mathrm{e}^{-2\xi_{1\mathfrak{I}}+2\xi_{2\mathfrak{I}}}),\\
&\xi_1 = -b_1 x + 2t + \frac{2y}{b_1}\mathrm{i}, \quad \xi_2 = -b_2 x + 2t + \frac{2y}{b_2}\mathrm{i}.
\end{aligned}$$

where

$$\begin{aligned}
r_1 &= \tfrac{1}{2}(b_1^2 + b_2^2)\sinh\left(2\xi_{2\mathfrak{R}}\right)\cosh^2\left(\xi_{1\mathfrak{R}}\right) - b_1 b_2\left[\cosh^2\left(\xi_{2\mathfrak{R}}\right) + \tfrac{1}{2}\right]\sinh\left(2\xi_{1\mathfrak{R}}\right) - b_1^2\sinh\left(2\xi_{2\mathfrak{R}}\right),\\
r_2 &= -b_2(b_1^2 + b_2^2)\sinh\left(\xi_{2\mathfrak{R}}\right)\cosh^3\left(\xi_{1\mathfrak{R}}\right) + b_1 b_2^2\sinh\left(2\xi_{1\mathfrak{R}}\right)\cosh\left(\xi_{1\mathfrak{R}}\right)\cosh\left(\xi_{2\mathfrak{R}}\right)\\
&\quad + 2b_1^2 b_2\sinh\left(\xi_{2\mathfrak{R}}\right)\cosh\left(\xi_{1\mathfrak{R}}\right) + b_1^3\sinh\left(\xi_{1\mathfrak{R}}\right)\cosh\left(\xi_{2\mathfrak{R}}\right),\\
r_3 &= b_1^2\sinh\left(\xi_{1\mathfrak{R}}\right)\left[b_1\cosh\left(\xi_{2\mathfrak{R}}\right)\mathrm{e}^{-6\xi_{1\mathfrak{I}}+5\xi_{2\mathfrak{I}}} - b_2\cosh\left(\xi_{1\mathfrak{R}}\right)\mathrm{e}^{-3\xi_{1\mathfrak{I}}+2\xi_{2\mathfrak{I}}}\right],\\
r_4 &= (b_1^2 + b_2^2)\sinh(\xi_{2\mathfrak{R}})\cosh^2(\xi_{1\mathfrak{R}}) - b_1 b_2\sinh(2\xi_{1\mathfrak{R}})\cosh(\xi_{2\mathfrak{R}}) - 2b_1^2\sinh(\xi_{2\mathfrak{R}}),\\
r_5 &= \mathrm{e}^{-\xi_{1\mathfrak{I}}+\xi_{2\mathfrak{I}}} + \mathrm{e}^{-3\xi_{1\mathfrak{I}}+3\xi_{2\mathfrak{I}}},\\
r_6 &= (b_1^2 + b_2^2)\cosh(\xi_{1\mathfrak{R}})\cosh(\xi_{2\mathfrak{R}}) - 2b_1 b_2\sinh(\xi_{1\mathfrak{R}})\sinh(\xi_{2\mathfrak{R}}).
\end{aligned}$$

To further investigate the composite and coexistence behaviors of different localized helical spin textures, we note that substituting (17) into (9) and (10) naturally leads to the coexistence of multiple spin textures. Due to the complexity of the analytic expressions of the corresponding wave functions and their integrals, a detailed derivation is not presented here. Nevertheless, by considering the following matrix relations, the three-component spin representation can still be obtained. Importantly, such coexistence does not arise from a linear superposition of individual spin textures, but instead originates from the nonlinear reconstruction induced by the gauge transformation. This guarantees that the resulting spin configurations remain self-consistent solutions of the underlying spin dynamics. Based on the Lax pair (2) and the gauge transformation procedure in Appendix A, spin textures possessing multiple excitation states can be constructed as follows:

$$\begin{aligned}
&\mathrm{S}[2] = \mathrm{S}[0] + 2\mathrm{i}\left[(\mathcal{H}_1)_x + (\mathcal{H}_2)_x\right],\\
&\mathrm{S}[3] = \mathrm{S}[0] + 2\mathrm{i}\left[(\mathcal{H}_1)_x + (\mathcal{H}_2)_x + (\mathcal{H}_3)_x\right],
\end{aligned} \tag{18}$$

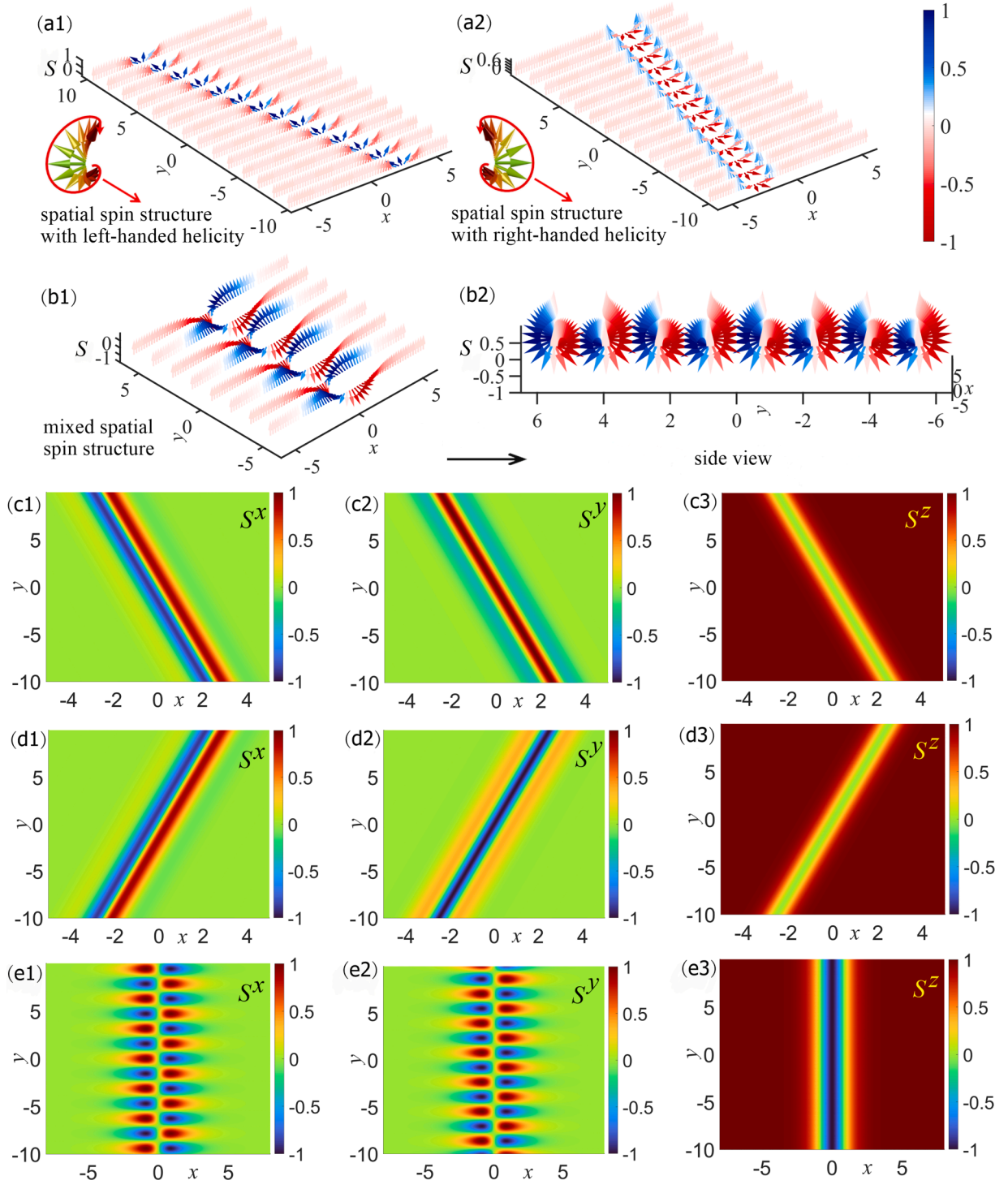

Fig. 2. (Color online) Basic localized helical spin textures with single-excitation states: panels (a1)-(b1) show the left-handed distribution, right-handed distribution, and mixed-type distribution, respectively, while panel (b2) presents the side view of the mixed-type configuration. The color band denotes the extent of bias along the $\pm y$ direction. During the time evolution, the three components constituting the localized helical spin textures form continuously varying localized wave structures. Panels (c1)-(c3), (d1)-(d3), and (e1)-(e3) respectively show the three-component distributions of the left-handed, right-handed, and mixed-type localized helical spin textures. The relevant parameters are: $\lambda_1|_{\text{Left}} = 2 - 2\text{i}$, $\lambda_1|_{\text{Right}} = -2 - 2\text{i}$, $\lambda_1|_{\text{Mixed}} = \text{i}$, and $u_0 = -v_1 = t = 0$.

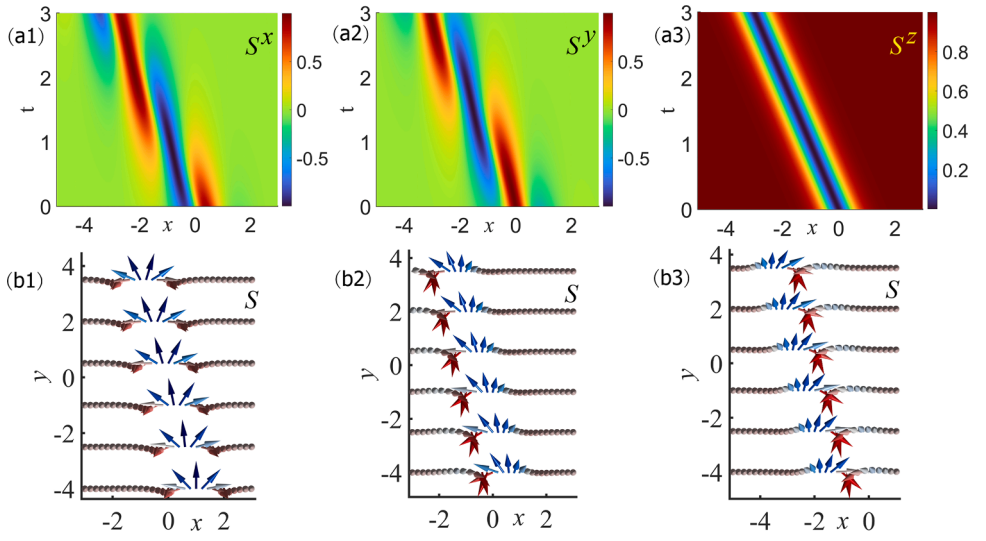

Fig. 3. (Color online) The inherent properties of the system lead to internal rotational characteristics induced by the superposition of chiral magnetic excitations and a uniformly rotating background. Under unchanged chirality, localized helical spin textures still exhibit markedly different spatiotemporal evolutions and spatial distribution characteristics. (a1)-(a3) Time evolutions of the three spin components at $y = 0$. The S^x and S^y components vary continuously in time, whereas the S^z component remains unchanged. (b1)-(b3) Spatial distributions of the spin textures at $t = 0$, 1, and 2, respectively, illustrate distinct spatial features despite identical chirality. In particular, at $t = \pi$, the spatial distribution recovers the same profile as that at $t = 0$, with an overall shift along the negative x direction. The relevant parameters are: $\lambda_1|_{\text{Left}} = 2 - 2\mathrm{i}$ and $u_0 = -\nu_1 = 0$.

with

$$\mathrm{S}[j] = \begin{pmatrix} S^{z[j]} & S^{x[j]} - \mathrm{i}S^{y[j]} \\ S^{x[j]} + \mathrm{i}S^{y[j]} & -S^{z[j]} \end{pmatrix}, \quad \mathcal{H}_N = \begin{pmatrix} \dfrac{\lambda_N^*|\phi_1^{[N-1]}|^2 + \lambda_N|\phi_2^{[N-1]}|^2}{(|\phi_1^{[N-1]}|^2 + |\phi_2^{[N-1]}|^2)|\lambda_N|^2} & \dfrac{(\lambda_N^* - \lambda_N)\phi_1^{[N-1]}\phi_2^{[N-1]*}}{(|\phi_1^{[N-1]}|^2 + |\phi_2^{[N-1]}|^2)|\lambda_N|^2} \\ \dfrac{(\lambda_N^* - \lambda_N)\phi_1^{[N-1]*}\phi_2^{[N-1]}}{(|\phi_1^{[N-1]}|^2 + |\phi_2^{[N-1]}|^2)|\lambda_N|^2} & \dfrac{\lambda_N|\phi_1^{[N-1]}|^2 + \lambda_N^*|\phi_1^{[N-1]}|^2}{(|\phi_1^{[N-1]}|^2 + |\phi_2^{[N-1]}|^2)|\lambda_N|^2} \end{pmatrix}.$$

In Eq. (18), the index $j = 0, 1, 2, \ldots, N$ and the subscript $N = 1, 2, 3, \ldots$, where [0] denotes the seed solution and $[j]$ represents the iterated solution containing j solitons. Based on Eq. (18), in order to further construct and analyze double-excitation bound states formed by localized helical spin textures with the same or opposite chirality, as well as multi-excitation coexistence configurations composed of basic localized helical spin textures, according to (12), we consider the background field $\vec{S} = (S^{x[0]}, S^{y[0]}, S^{z[0]}) = (0, 0, 1)$, and take $u = u_0$. Under this background, the eigenfunction of Eq. (2) can be obtained as:

$$\Phi = \begin{pmatrix} \phi_1 \\ \phi_2 \end{pmatrix} = \begin{pmatrix} f_1\left(\frac{\lambda t+y}{\lambda}\right)\mathrm{e}^{-\frac{1}{2}\mathrm{i}(\nu_1+u_0)y}\mathrm{e}^{\frac{1}{2}\mathrm{i}\lambda x} \\ f_2\left(\frac{\lambda t+y}{\lambda}\right)\mathrm{e}^{\frac{1}{2}\mathrm{i}(\nu_1+u_0)y}\mathrm{e}^{-\frac{1}{2}\mathrm{i}\lambda x} \end{pmatrix}, \tag{19}$$

where the $f_1(\frac{\lambda t+y}{\lambda}) = \mathrm{e}^{\frac{\lambda t+y}{\lambda}}$ and $f_2(\frac{\lambda t+y}{\lambda}) = \mathrm{e}^{-\frac{\lambda t+y}{\lambda}}$ represent arbitrary functions. Using the gauge transformation procedure in Appendix A, the multi-excitation states for Eq. (1) can be constructed as:

$$S^{x[j]} = S^{x[j-1]} + \kappa_1, \; S^{y[j]} = S^{y[j-1]} + \kappa_2, \; S^{z[j]} = S^{z[j-1]} + \kappa_3, \; u^{[j]} = \frac{S^{z[j-1]}}{S^{z[j]}}u_{j-1} + \kappa_4, \tag{20}$$

with

$$\kappa_1 = \frac{\mathrm{i}\Big\{[(\phi_1^{[j-1]})^2 - (\phi_2^{[j-1]})^2][(\phi_{1x}^{[j-1]})^*(\phi_2^{[j-1]})^* - (\phi_1^{[j-1]})^*(\phi_{2x}^{[j-1]})^*] + [(\phi_1^{[j-1]*})^2 - (\phi_2^{[j-1]*})^2][\phi_2^{[j-1]}\phi_{1x}^{[j-1]} - \phi_1^{[j-1]}\phi_{2x}^{[j-1]}]\Big\}(\lambda_j - \lambda_j^*)}{|\lambda_j|^2(|\phi_1^{[j-1]}|^2 + |\phi_2^{[j-1]}|^2)^2},$$

$$\kappa_2 = \frac{\Big\{[(\phi_1^{[j-1]})^2 + (\phi_2^{[j-1]})^2][(\phi_1^{[j-1]})^*(\phi_{2x}^{[j-1]})^* - (\phi_{1x}^{[j-1]})^*(\phi_2^{[j-1]})^*] + [(\phi_1^{[j-1]*})^2 + (\phi_2^{[j-1]*})^2][\phi_2^{[j-1]}\phi_{1x}^{[j-1]} - \phi_1^{[j-1]}\phi_{2x}^{[j-1]}]\Big\}(\lambda_j - \lambda_j^*)}{|\lambda_j|^2(|\phi_1^{[j-1]}|^2 + |\phi_2^{[j-1]}|^2)^2},$$

$$\kappa_3 = -\frac{2\mathrm{i}\Big\{[\phi_1^{[j-1]}\phi_2^{[j-1]}][(\phi_{1x}^{[j-1]})^*(\phi_2^{[j-1]})^* - (\phi_1^{[j-1]})^*(\phi_{2x}^{[j-1]})^*] + [(\phi_1^{[j-1]})^*(\phi_2^{[j-1]})^*][\phi_2^{[j-1]}\phi_{1x}^{[j-1]} - \phi_1^{[j-1]}\phi_{2x}^{[j-1]}]\Big\}(\lambda_j - \lambda_j^*)}{|\lambda_j|^2(|\phi_1^{[j-1]}|^2 + |\phi_2^{[j-1]}|^2)^2},$$

$$\kappa_4 = \frac{\Big\{\nu_1(S^{z[0]} - S^{z[1]})(|\phi_1^{[j-1]}|^2 + |\phi_2^{[j-1]}|^2)^2|\lambda_j|^2 + 2\mathrm{i}(\lambda_j - \lambda_j^*)[|\phi_1^{[j-1]}|^2[(\phi_2^{[j-1]})^*\phi_2^{[j-1]}]_t - |\phi_2^{[j-1]}|^2[(\phi_1^{[j-1]})^*\phi_1^{[j-1]}]_t]\Big\}}{S^{z[j]}|\lambda_j|^2(|\phi_1^{[j-1]}|^2 + |\phi_2^{[j-1]}|^2)^2}.$$

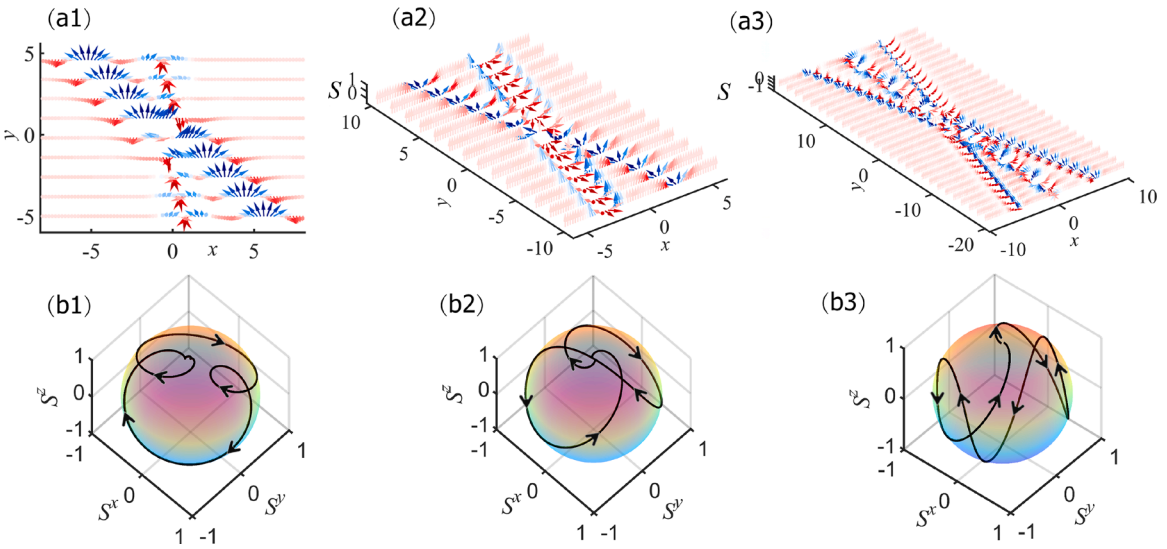

Fig. 4. (Color online) Multi-excitation coexistence configurations formed by basic localized helical spin textures. Panels (a1)-(a3) respectively show a bound state formed by two left-handed textures, the coexistence of left-handed and right-handed textures, and the simultaneous coexistence of three types of basic localized helical spin textures; panels (b1)-(b3) present the trajectories of the three spin-texture components on the Bloch sphere, which geometrically confirm the corresponding chiral coexistence features.

According to (2) and Appendix A, when $j = 1$ or 2, the corresponding eigenfunctions are given by $(\phi_1^{[0]}, \phi_2^{[0]})^{\mathrm{T}} = (\phi_1|_{\lambda=\lambda_1}, \phi_2|_{\lambda=\lambda_1})^{\mathrm{T}}$ and $(\phi_1^{[1]}, \phi_2^{[1]})^{\mathrm{T}} = (\frac{1}{\lambda_2} I - H_1 \Lambda_1^{-1} H_1^{-1})(\phi_1|_{\lambda=\lambda_2}, \phi_2|_{\lambda=\lambda_2})^{\mathrm{T}}$. Based on Eqs. (19) and (20), when $j = 1$, the basic localized helical spin texture in the single-excitation state can be recovered, corresponding to the structure described by Eq. (12). When $j = 2$, the localized helical spin texture with a double-excitation state can be further constructed, whose analytical form remains consistent with the first expression in Eq. (18). Furthermore, the spin textures corresponding to double-excitation bound states with identical and opposite chirality can be obtained, as shown in Fig. 4(a1) and (a2). When $j = 3$, a multi-excitation coexistence configuration composed of basic localized helical spin textures can be obtained, as shown in Fig. 4(a3).

These results demonstrate that, within the gauge-equivalence framework, localized helical spin textures induced by analytical solutions of the scalar field equation can exist not only as isolated excitations but also form stable composite and coexisting states while preserving their intrinsic helical characteristics. The bound and coexisting configurations associated with different chirality combinations essentially reflect the reconstruction of the spatial structure of the spin field under gauge transformations in the presence of multimode wave functions. Therefore, the analysis presented in this section does not rely on introducing additional spin interactions; instead, it reveals the superposability and composability of localized helical spin textures in two-dimensional ferromagnetic systems from an analytical-structural perspective, providing a unified construction scheme for systematically characterizing more complex spin configurations.

It is worth emphasizing that the localized helical spin textures reported here are fundamentally different from several well-known magnetic textures, including skyrmions, conventional magnetic solitons, and helical states in chiral magnets [34,35]. Skyrmions are characterized primarily by nontrivial topological spin wrapping, where the spin configuration continuously evolves from a nearly uniform background toward a reversed core region, thereby forming a finite topological charge [34,36]. Conventional magnetic solitons, by contrast, mainly describe localized nonlinear magnetization excitations embedded in a nearly uniform magnetic background [7,37], whose essential feature is spatial localization rather than intrinsic continuous helical rotation. Magnetic vortices typically exhibit circulating in-plane spin configurations surrounding a localized vortex core [38,39], where the rotational behavior is concentrated around the core region. In addition, the helical states commonly observed in chiral magnets correspond to spatially extended periodic spiral magnetic orders stabilized by the Dzyaloshinskii-Moriya interaction [40,41]. By contrast, the localized helical spin textures constructed in the present work represent spatially localized nonlinear chiral excitations characterized by continuously distributed helical rotational behavior confined within a finite spatial region. Their chirality does not originate from topological protection or antisymmetric exchange interactions, but instead emerges dynamically from the intrinsic nonlinear rotational evolution of the two-dimensional spin field itself.

4. Conclusion and discussion

In this work, we have investigated a class of localized helical spin textures within a continuous spin-dynamical framework for two-dimensional ferromagnetic systems. By employing the gauge-equivalence formulation between the spin field equation and an analytically solvable scalar equation, we explicitly reconstructed full three-component spin configurations in real space and analyzed their spatial structures in a systematic manner.

Within this framework, we identified three fundamental types of localized helical spin textures: left-handed, right-handed, and mixed helices. These textures are spatially localized while exhibiting continuous internal spin rotation, and their helical characteristics are quantified through the polar and azimuthal angle representation of the spin field. A local chirality criterion based on the phase-gradient flow of the azimuthal angle was introduced, providing a direct and intrinsic measure to distinguish different helical handedness without invoking topological invariants or additional chiral interactions.

Furthermore, the spatial evolution of the spin textures reveals that the continuous structural variation of the transverse spin components originates from the interplay between localized chiral excitations and the uniformly distributed background phase rotation. This mechanism leads to periodic structural modulation during time evolution, while preserving the overall localization of the spin texture.

Beyond individual textures, we demonstrated that multiple localized helical spin textures can coexist and form composite configurations through nonlinear reconstruction within the gauge-equivalent framework. These composite states remain self-consistent solutions of the original spin model and exhibit distinct structural features depending on the chirality of their constituent textures.

Overall, the present results highlight localized helical spin textures as a class of fundamental nonlinear excitations in two-dimensional ferromagnetic systems. The gauge-equivalence approach adopted here provides a transparent analytical route for characterizing their spatial structure, chirality, and evolution, offering a complementary perspective to conventional studies focused on periodic or topologically protected magnetic textures.

It should be emphasized that the chirality discussed in this work differs fundamentally from the conventional chiral structures induced by Dzyaloshinskii-Moriya interactions. Here, the chiral structures emerge in a system governed solely by Heisenberg exchange interactions, where chirality is defined through the integral of the phase-gradient flow associated with the spin configuration. The direction of the overall phase evolution determines the corresponding chirality type. Such chiral structures remain stable only under dynamical evolution and therefore differ from the ground-state chiral textures typically found in DMI-driven spiral magnets. Instead, they represent a special class of excited chiral states sustained by nonlinear dynamics in Heisenberg ferromagnets [42–45].

After obtaining the exact solution of this two-dimensional helical spin state, we further examined its stability under several physical conditions. Our numerical results show that this structure undergoes deformation and eventual breakup in the presence of random perturbations and external magnetic fields, suggesting that it may be difficult to observe experimentally.

Several open issues naturally follow from the present study. For instance, extending the present framework to include additional interactions or anisotropies may further enrich the variety of localized chiral spin states. We expect that the analytical framework developed here will provide a useful starting point for future investigations of localized spin textures and their collective behaviors in high-dimensional magnetic systems.

CRediT authorship contribution statement

Xiao-Qi Cui: Writing – review & editing, Writing – original draft, Visualization, Validation, Software, Methodology, Investigation, Data curation; **Xin-Wei Jin:** Writing – review & editing, Methodology, Funding acquisition, Formal analysis; **Shiyi Wang:** Writing – review & editing, Visualization, Methodology; **Xiao-Yong Wen:** Writing – review & editing, Funding acquisition; **Zhan-Ying Yang:** Writing – review & editing, Supervision, Project administration, Funding acquisition.

Data availability

Data will be made available on request.

Declaration of competing interest

The authors declare that they have no financial and personal relationships with other people or organizations that can inappropriately influence our work, there is no professional or other personal interest of any nature or kind in any product, service and/or company that could be construed as influencing the position presented in, or the review of, the manuscript entitled “Localized helical spin texture in ferromagnetic thin films”.

Acknowledgement

We thank the other members of the discussion group for their valuable comments.

Funding

This research was supported by Zhejiang Provincial Natural Science Foundation of China under Grant No. LQN25A050002, and the National Natural Science Foundation of China (Grant Nos. 12275213, 12247103, 12571263, 12505009, 12071042), and Beijing Natural Science Foundation (Grant No. 1242004).

Appendix A. The iterative N-fold DT of Eq. (3)

For Eq. (3) and its Lax pair (4), we select the seed solution $\psi_0 = 0$ from which the corresponding eigenfunctions can be obtained as

$$\Psi = \begin{pmatrix} \varphi_1 \\ \varphi_2 \end{pmatrix} = \begin{pmatrix} f_1\left(\frac{\lambda t+y}{\lambda}\right)e^{\frac{1}{2}i\lambda x} \\ f_2\left(\frac{\lambda t+y}{\lambda}\right)e^{-\frac{1}{2}i\lambda x} \end{pmatrix}, \tag{A.1}$$

where the f_1 and f_2 are arbitrary functions related to λ, y and t. Next, starting from the gauge transformation $\widetilde{\Psi} = T\Psi$, the transformation matrix T must satisfy the following compatibility conditions:

$$T_x + TU - \widetilde{U}T = 0, \quad T_t + TV - \widetilde{V}T - \lambda T_y = 0. \tag{A.2}$$

We introduce the matrices T and Ψ as

$$\begin{aligned} &T = T^{[\iota]} = \lambda I - H_\iota \Lambda_\iota H_\iota^{-1}, \quad (\iota = 1, 2, \ldots, N), \\ &\Psi^{[\iota]} = (T^{[\iota-1]}T^{[\iota-2]}\ldots T^{[1]})|_{\lambda=\lambda_\iota}\Psi, \quad \Psi^{[\iota-1]} = (\varphi_1^{[\iota-1]}, \varphi_2^{[\iota-1]})^T, \end{aligned} \tag{A.3}$$

where $I = diag(1, 1)$, the matrices Λ_ι and H_ι are expressed as:

$$\Lambda_\iota = \begin{pmatrix} \lambda_\iota & 0 \\ 0 & \lambda_\iota^* \end{pmatrix}, \quad H_\iota = \begin{pmatrix} f_\iota^{\iota-1} & (g_\iota^{\iota-1})^* \\ g_\iota^{\iota-1} & -(f_\iota^{\iota-1})^* \end{pmatrix}.$$

By applying (4), (A.1)–(A.3), setting $\iota = 1$ gives the 1-fold DT:

$$\begin{aligned} &\Psi^{[1]} = T^{[1]}\Psi^{[0]} = (\lambda I - H_1\Lambda_1 H_1^{-1})\Psi^{[0]}, \\ &\psi_1 = \psi_0\left[\frac{\lambda_1^*\left|g_1^0\right|^2 + \left|f_1^0\right|^2\lambda_1}{\lambda_1^*\left|f_1^0\right|^2 + \left|g_1^0\right|^2\lambda_1}\right] - \frac{(\chi_1 - \chi_2 + \chi_3 - \chi_4)(\lambda_1^* - \lambda_1)}{\left(\left|f_1^0\right|^2 + \left|g_1^0\right|^2\right)\left(\lambda_1^*\left|f_1^0\right|^2 + \left|g_1^0\right|^2\lambda_1\right)}, \end{aligned}$$

with

$$\chi_1 = (f_1^0)^*(f_1^0)^2\left[(g_1^0)_x\right]^*, \ \chi_2 = f_1^0(g_1^0)_x\left[(g_1^0)^2\right]^*, \ \chi_3 = g_1^0(f_1^0)_x\left[(g_1^0)^2\right]^*, \ \chi_4 = (g_1^0)^*(f_1^0)^2\left[(f_1^0)_x\right]^*.$$

Here, $\Psi^{[0]} = (f_1^0, g_1^0)^T = (\varphi_1|_{\lambda=\lambda_1}, \varphi_2|_{\lambda=\lambda_1})^T$. By taking $\iota = 2$, the 2-fold DT can be expressed as

$$\begin{aligned} &\Psi^{[2]} = T^{[2]}\Psi^{[1]} = (\lambda I - H_2\Lambda_2 H_2^{-1})T^{[1]}\Psi^{[0]}, \\ &\psi_2 = \psi_1\left[\frac{\lambda_2^*\left|g_2^1\right|^2 + \left|f_2^1\right|^2\lambda_2}{\lambda_2^*\left|f_2^1\right|^2 + \left|g_2^1\right|^2\lambda_2}\right] - \frac{(\chi_1 - \chi_2 + \chi_3 - \chi_4)(\lambda_2^* - \lambda_2)}{\left(\left|f_2^1\right|^2 + \left|g_2^1\right|^2\right)\left(\lambda_2^*\left|f_2^1\right|^2 + \left|g_2^1\right|^2\lambda_2\right)}, \end{aligned}$$

where $\Psi^{[1]} = (f_2^1, g_2^1)^T = (\lambda_2 I - H_1\Lambda_1 H_1^{-1})(\varphi_1|_{\lambda=\lambda_2}, \varphi_2|_{\lambda=\lambda_2})^T$. By repeating this iterative process, the general form of the N-fold DT can be obtained.

Theorem. Let $\Psi^{[\iota-1]} = (\varphi_1|_{\lambda=\lambda_\iota}, \varphi_2|_{\lambda=\lambda_\iota})^T$ be N eigenfunction of Lax pair (4) with λ_ι ($\iota = 1, 2, \ldots, N$), ψ_0 is a seed solutions of Eq. (3), the iterative N-fold DT can be written as

$$\begin{aligned} &\Psi^{[N]} = T\Psi^{[0]}, \\ &\psi_N = \psi_{N-1}\left[\frac{\lambda_N^*\left|g_N^{N-1}\right|^2 + \left|f_N^{N-1}\right|^2\lambda_N}{\lambda_N^*\left|f_N^{N-1}\right|^2 + \left|g_N^{N-1}\right|^2\lambda_N}\right] - \frac{(\chi_1 - \chi_2 + \chi_3 - \chi_4)(\lambda_N^* - \lambda_N)}{\left(\left|f_N^{N-1}\right|^2 + \left|g_N^{N-1}\right|^2\right)\left(\lambda_N^*\left|f_N^{N-1}\right|^2 + \left|g_N^{N-1}\right|^2\lambda_N\right)}, \\ &\chi_1 = (f_N^{N-1})^*(f_N^{N-1})^2\left[(g_N^{N-1})_x\right]^*, \quad \chi_2 = \left[(g_N^{N-1})^2\right]^* f_N^{N-1}(g_N^{N-1})_x, \\ &\chi_3 = \left[(g_N^{N-1})^2\right]^* g_N^{N-1}(f_N^{N-1})_x, \qquad \chi_4 = (g_N^{N-1})^*(f_N^{N-1})^2\left[(f_N^{N-1})_x\right]^*. \end{aligned} \tag{A.4}$$

where $T = R_N R_{N-1}\ldots R_0$, $R_\iota = T_\iota^{[v_\iota+1]}\ldots T_\iota^{[1]}$ ($\iota = 1, 2, \ldots, N$), $\Psi_\iota[0] = (R_{\iota-1}\ldots R_0)|_{\lambda=\lambda_\iota}\Psi^{[0]}$, $R_0 = I$, in which

$$T_\iota^{[q]} = \lambda I - Q_\iota[q] = \begin{pmatrix} \lambda - Q_{11\iota}[q] & -Q_{12\iota}[q] \\ -Q_{21\iota}[q] & \lambda - Q_{22\iota}[q] \end{pmatrix},$$

where

$$\begin{aligned} &Q_{11\iota}[q] = \frac{(\lambda - \lambda_\iota)|f_\iota^{[q-1]}|^2 - |g_\iota^{[q-1]}|^2(\lambda_\iota^* - \lambda)}{|f_\iota^{[q-1]}|^2 + |g_\iota^{[q-1]}|^2}, \quad Q_{12\iota}[q] = \frac{(\lambda_\iota^* - \lambda_\iota)f_\iota^{[q-1]}g_\iota^{[q-1]*}}{|f_\iota^{[q-1]}|^2 + |g_\iota^{[q-1]}|^2}, \\ &Q_{21\iota}[q] = \frac{(\lambda_\iota^* - \lambda_\iota)f_\iota^{[q-1]*}g_\iota^{[q-1]}}{|f_\iota^{[q-1]}|^2 + |g_\iota^{[q-1]}|^2}, \quad Q_{22\iota}[q] = \frac{|g_\iota^{[q-1]}|^2(\lambda - \lambda_\iota) - (\lambda_\iota^* - \lambda)|f_\iota^{[q-1]}|^2}{|f_\iota^{[q-1]}|^2 + |g_\iota^{[q-1]}|^2}, \end{aligned}$$

and $q = 1, 2, \ldots, N$.

References

[1] M.N. Tey, X. Chen, A. Soumyanarayanan, P. Ho, Chiral spin textures for next-generation memory and unconventional computing, ACS Appl. Electron. Mater. 4 (11) (2022) 5088–5097.
[2] A. Bogdanov, A. Hubert, Thermodynamically stable magnetic vortex states in magnetic crystals, J. Magn. Magn. Mater. 138 (3) (1994) 255–269.
[3] S. Emori, U. Bauer, S.M. Ahn, E. Martinez, G.S. Beach, Current-driven dynamics of chiral ferromagnetic domain walls, Nat. Mater. 12 (7) (2013) 611–616.
[4] D. Gosálbez-Martínez, A. Crepaldi, O.V. Yazyev, Diversity of radial spin textures in chiral materials, Phys. Rev. B 108 (20) (2023) L201114.
[5] Z. Ying, Z.L. Li, B.G. Shen, Research progress in the magnetic domain wall topology, Acta Phys. Sin. 73 (1) (2024) 017504.
[6] K. Wang, V. Bheemarasetty, J. Duan, S. Zhou, G. Xiao, Fundamental physics and applications of skyrmions: a review, J. Magn. Magn. Mater. 563 (2022) 169905.
[7] A.M. Kosevich, B.A. Ivanov, A.S. Kovalev, Magnetic solitons, Phys. Rep. 194 (3-4) (1990) 117–238.
[8] N. Papanicolaou, T.N. Tomaras, Dynamics of magnetic vortices, Nucl. Phys. B 360 (2-3) (1991) 425–462.
[9] A.A. Thiele, Steady-state motion of magnetic domains, Phys. Rev. Lett. 30 (6) (1973) 230.
[10] S.E. Barnes, S. Maekawa, Generalization of Faraday's law to include nonconservative spin forces, Phys. Rev. Lett. 98 (24) (2007) 246601.
[11] J. Zang, M. Mostovoy, J.H. Han, N. Nagaosa, Dynamics of skyrmion crystals in metallic thin films, Phys. Rev. Lett. 107 (13) (2011) 136804.
[12] K. Everschor-Sitte, Rotating skyrmion lattices by spin torques and field or temperature gradients, in: Spintronics: Progress in Theory, Materials, and Devices, 2013, p. 50.
[13] Y. Tserkovnyak, J. Xiao, Energy storage via topological spin textures, Phys. Rev. Lett. 121 (12) (2018) 127701.
[14] Y. Zhou, S. Li, X. Liang, Y. Zhou, Topological spin textures: basic physics and devices, Adv. Mater. 37 (2) (2025) 2312935.
[15] L.A. L.E. Landau, E. Lifshitz, On the theory of the dispersion of magnetic permeability in ferromagnetic bodies, in: Perspectives in Theoretical Physics, Pergamon, 1992, pp. 51–65.
[16] L.A. Takhtajan, Integration of the continuous Heisenberg spin chain through the inverse scattering method, Phys. Lett. A 64 (2) (1977) 235–237.
[17] S.W. Cheong, X. Xu, Magnetic chirality, NPJ Quantum Mater. 7 (1) (2022) 40.
[18] X. W. Jin, Y. Liu, Z. Y. Yang, Z. M. Liao, G. Jing, W. L. Yang, Hidden chiral mode self-generated from intrinsic magnetic heterogeneity, Phys. Rev. B, 110 (18), (2024) 184424.
[19] U. K. Roessler, A. N. Bogdanov, C. Pfleiderer, Spontaneous skyrmion ground states in magnetic metals, Nature, 442 (7104), (2006) 797–801.
[20] M. Garst, J. Waizner, D. Grundler, Collective spin excitations of helices and magnetic skyrmions: review and perspectives of magnonics in non-centrosymmetric magnets, J. Phys. D Appl. Phys. 50 (29) (2017) 293002.
[21] H. Yu, J. Xiao, H. Schultheiss, Magnetic texture based magnonics, Phys. Rep. 905 (2021) 1–59.
[22] R. Takagi, D. Morikawa, K. Karube, N. Kanazawa, K. Shibata, G. Tatara, S. Seki, Spin-wave spectroscopy of the Dzyaloshinskii-Moriya interaction in room-temperature chiral magnets hosting skyrmions, Phys. Rev. B 95 (22) (2017) 220406.
[23] Y. Cao, Z. Huang, Y. Yin, H. Xie, B. Liu, W. Wang, W. Huang, Overview and advances in a layered chiral helimagnet Cr1/3NbS2, Mater. Today Adv. 7 (2020) 100080.
[24] B. Ding, J. Liu, H. Li, J. Liang, J. Chen, Z. Li, W. Wang, Observation of short-period helical spin order and magnetic transition in a nonchiral centrosymmetric helimagnet, Adv. Funct. Mater. 32 (19) (2022) 2200356.
[25] R. Myrzakulov, G. Mamyrbekova, G. Nugmanova, M. Lakshmanan, Integrable (2 + 1)-dimensional spin models with self-consistent potentials, Symmetry 7 (3) (2015) 1352–1375.
[26] Z.H. Zhang, M. Deng, W.Z. Zhao, K. Wu, On the (2 + 1)-dimensional integrable inhomogeneous Heisenberg ferromagnet equation, J. Phys. Soc. Jpn. 75 (10) (2006) 104002.
[27] X.Q. Cui, L. Duan, X.W. Jin, X.Y. Wen, Z.Y. Yang, Spontaneous switching dynamics of magnetic soliton structures in two-dimensional spin systems, Chaos Solitons Fractals 201 (2025) 117235.
[28] X.W. Jin, J. Lin, Rogue wave, interaction solutions to the KMM system, J. Magn. Magn. Mater. 502 (2020) 166590.
[29] J. Lin, B. Ren, H.M. Li, Y.S. Li, Soliton solutions for two nonlinear partial differential equations using a Darboux transformation of the Lax pairs, Phys. Rev. E-Stat. Nonlinear Soft Matter Phys. 77 (3) (2008) 036605.
[30] X. Zhu, Gauge equivalent structures of the integrable (2 + 1)-dimensional nonlocal nonlinear Schrödinger equations and their applications, Phys. Scr. 98 (7) (2023) 075203.
[31] R. Myrzakulov, S. Vijayalakshmi, G.N. Nugmanova, M. Lakshmanan, A (2 + 1)-dimensional integrable spin model: geometrical and gauge equivalent counterpart, solitons and localized coherent structures, Phys. Lett. A 233 (4–6) (1997) 391–396.
[32] M. Lakshmanan, R. Myrzakulov, S. Vijayalakshmi, A.K. Danlybaeva, Motion of curves and surfaces and nonlinear evolution equations in (2 + 1) dimensions, J. Math. Phys. 39 (7) (1998) 3765–3771.
[33] R. Myrzakulov, S. Vijayalakshmi, R.N. Syzdykova, M. Lakshmanan, On the simplest (2 + 1) dimensional integrable spin systems and their equivalent nonlinear Schrödinger equations, J. Math. Phys. 39 (4) (1998) 2122–2140.
[34] N. Nagaosa, Y. Tokura, Topological properties and dynamics of magnetic skyrmions, Nat. Nanotechnol. 8 (12) (2013) 899–911.
[35] I. Makhfudz, B. Krüger, O. Tchernyshyov, Inertia and chiral edge modes of a skyrmion magnetic bubble, Phys. Rev. Lett. 109 (21) (2012) 217201.
[36] W. Jiang, X. Zhang, G. Yu, et al., Direct observation of the skyrmion Hall effect, Nat. Phys. 13 (2) (2017) 162–169.
[37] B.A. Ivanov, V.A. Stephanovich, Two-dimensional solitons in magnets, Phys. Lett. A 141 (1–2) (1995) 89–94.
[38] T. Shinjo, T. Okuno, R. Hassdorf, et al., Magnetic vortex core observation in circular dots of permalloy, Science 289 (5481) (2000) 930–932.
[39] A. Wachowiak, J. Wiebe, M. Bode, et al., Direct observation of internal spin structure of magnetic vortex cores, Science 298 (5593) (2002) 577–580.
[40] S. Mühlbauer, B. Binz, F. Jonietz, et al., Skyrmion lattice in a chiral magnet, Science 323 (5916) (2009) 915–919.
[41] X.Z. Yu, Y. Onose, N. Kanazawa, et al., Real-space observation of a two-dimensional skyrmion crystal, Nature 465 (7300) (2010) 901–904.
[42] K.W. Kim, H.W. Lee, K.J. Lee, M.D. Stiles, Chirality from interfacial spin-orbit coupling effects in magnetic bilayers, Phys. Rev. Lett. 111 (21) (2013) 216601.
[43] M.M. Valizadeh, S. Satpathy, Dzyaloshinskii-Moriya interaction in the presence of Rashba and Dresselhaus spin-orbit coupling, Phys. Rev. B 97 (2018) 094419.
[44] R. Cardias, A. Bergman, A. Szilva, Y.O. Kvashnin, J. Fransson, A.B. Klautau, O. Eriksson, L. Nordström, Dzyaloshinskii-Moriya interaction in absence of spin-orbit coupling, 2020, arXiv:2003.04680
[45] H. Pérez Rojas, E. Rodríguez Querts, Chiral current generation in QED by longitudinal photons, Nucl. Phys. B 909 (2016) 230–242.